Accurately Measured Precipitate–Matrix Misfit in an Al–Mg–Si Alloy by Electron Microscopy

Sigurd Wenner[a]* and Randi Holmestad[a]

[a]Department of Physics, NTNU, Høgskoleringen 5, NO-7491 Trondheim, Norway
*Phone: +47 73594197 Fax: +47 73591410 E-mail: sigurd.wenner@ntnu.no

Abstract

The age-hardenable Al–Mg–Si alloy system is strengthened by needle-shaped coherent β'' phase precipitates. Using distortion-corrected high-resolution scanning transmission electron microscopy images, we measure the considerable misfit between β'' particles and the Al matrix. The β'' phase is found to adapt its lattice parameters to the particle shape, distributing the strain in the Al matrix evenly in its cross-sectional plane. The measured misfits give a good match to reported atomistic simulations for a β'' phase with composition $Mg_5Al_2Si_4$.

Keywords: electron microscopy, aluminium alloys, precipitation, misfit strain
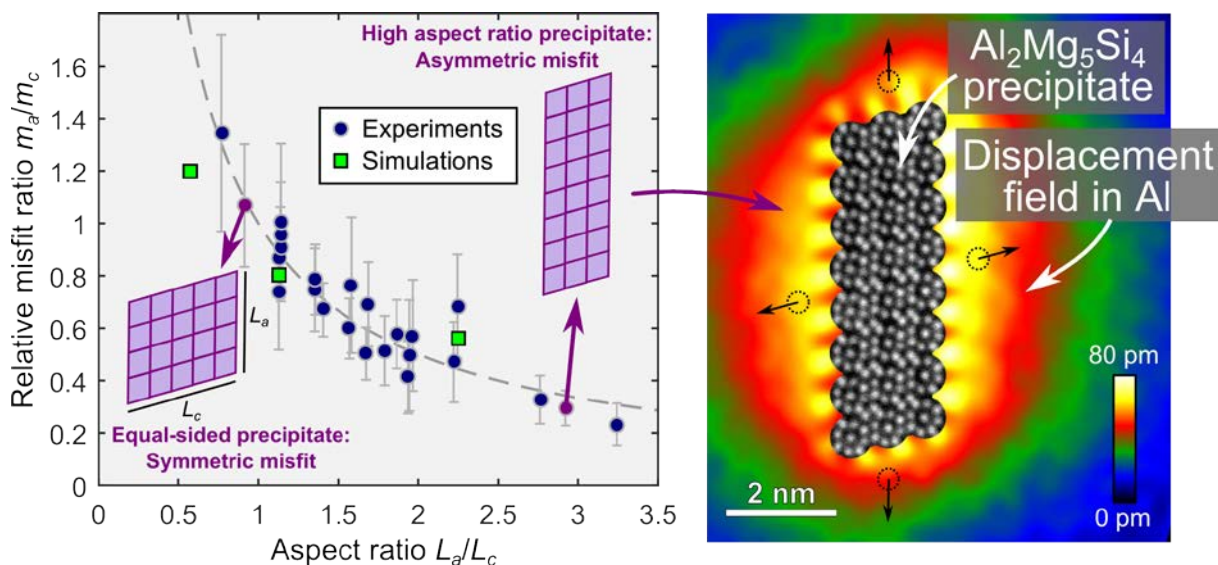
Coherent precipitates in age hardenable alloys and the misfit strain fields they induce in the surrounding matrix have been text book material for many decades [1]. Such precipitates form by thermally activated diffusion, nucleation and growth. A precipitate particle stays coherent until it grows too large for the matrix to accommodate all its misfit. After this, precipitates experience a loss of coherency, and the strain fields diminish, weakening the material. This can happen through several mechanisms:

- (i)   a phase transformation to a less coherent phase
- (ii) formation of an incoherent surface layer at the matrix-precipitate interface
- (iii) introduction of interface (misfit) dislocations

The precipitate phase can also relieve the system of some strain *before* coherency loss occurs by less drastic modifications:

- (iv) generation of stacking faults in the precipitate phase
- (v)   chemical adjustments, including an increased vacancy density in or outside the precipitate phase

All five effects can be studied using theoretical calculations such as density functional theory (DFT) or continuum mechanics through the finite element method (FEM). However, calculations need support by experiments at the atomic scale. Experimental studies require that we can both observe the causes (e.g. a single stacking fault) and quantify the resulting change in lattice strain. It is equally important to ensure the *absence* of faults, if the strain around a perfectly coherent particle is of interest.

In this study, we focus on measuring the misfit of perfectly coherent β'' precipitates of the Al–Mg–Si system [2–4] through scanning transmission electron microscopy (STEM). This phase is described by the monoclinic *C2/m* space group and was initially thought to have composition Mg_5Si_6, but $Mg_5Al_2Si_4$ is probably closer to the truth [5,6]. Its lattice parameters have been measured to $a = 1.516$ nm, $b = 0.405$ nm, $c = 0.674$ nm, and its monoclinic angle is 105.3° [2,3]. The phase was chosen since it is one of few fully coherent phases in aluminium alloys, and the main hardening phase of an industrially important alloy system. It is also needle-shaped with a long main coherency direction, often extending through the TEM specimen in which it resides. The lattice strain is therefore uniform through the specimen, and can be measured reliably in a projected image of a precipitate cross-section.

When corrected for spherical aberrations, annular dark-field STEM (ADF-STEM) can resolve all atomic lattices with spacings greater than ~0.1 nm, and give readily interpretable images that tell the microscopist where an atomic column is and how heavy its atoms are [7]. Unfortunately, this otherwise superb imaging technique is plagued by scan distortions related to probe flyback, specimen drift, electronic noise and other environmental effects [8,9]. Accurate atomic positions are required for high-resolution strain measurements, and experimenters therefore typically resort to conventional high-resolution TEM imaging [10,11] or only measuring strain along the fast-scan direction in a STEM image when high precision is required. Lower-resolution strain maps can be obtained by e.g. dark field imaging [12], dark-field holography [11] or (convergent) electron beam diffraction [13]. But hope is not lost for ADF-STEM: A methodology based on multi-frame exposures and alignment of the scan rows in each frame has proven to increase the positional accuracy up to the level of conventional TEM [14], without suffering effects such as uneven focus and contrast reversal. We apply the multi-frame STEM methodology to our problem to accurately extract the position of each atomic column, whether inside the precipitate or in the Al matrix outside it. The advantage over many other strain measurement techniques [13] is that all details on e.g. interfaces and defects are also observable in the image which is used for strain mapping.

With STEM being a technique of projection, the current treatment is two-dimensional, and the strain/misfit in the *b* ($[010]_{β''}$) direction is not measured. These values are however close to zero as the precipitates grow very long (30–150 nm for our material) in this direction. Indeed, zero *b*-misfit is enforced in the simulations we compare our results with [6,15,16].

A low-solute alloy was studied, with nominal composition (weight fraction) 0.37% Mg, 0.45% Si, 0.03% Mn, 0.20% Fe, and the remainder Al. The material was solution heat treated at 535 °C and aged at 195 °C for 4 hours (more details in Ref. [17]). Specimens were electropolished from thin foils, using a Struers TenuPol-5 and 1/3 nitric acid in 2/3 methanol kept at −25 °C. ADF-STEM image series were acquired on a double corrected JEOL ARM-200F with a cold field emission gun. The acceleration voltage was set to 80 kV to avoid damaging the specimen during the ~5 minute long acquisitions. A beam current of 6.5 pA was measured. The beam convergence angle was 27 mrad and the collection angles of the ADF detector were 35–149 mrad. The electron beam was parallel to $[010]_{\beta''}$ axes, which are oriented along $<001>_{Al}$.

Each image series consisted of about 30 images with 2048×2048 pixels and a 30×30 nm scan area. Images were aligned and non-rigidly registered using Smart Align [9], reducing the flyback distortions by a factor of about 5, when comparing the series average to a typical single frame ADF image. Geometric phase analysis (GPA) [18] was used to find displacement and strain fields by applying a cosine mask to $[200]_{Al}$ and $[020]_{Al}$ Fourier spots. The fields were calibrated by linear fitting, setting the average displacement to zero along distortion-free image boundaries. The displacement fields were compared to those found by a real-space approach consisting of atomic column positioning by peak finding, producing highly consistent results (see also [14]).

The choice of GPA as a main method comes from its swift processing route and its flexibility in prioritizing real-space resolution or reciprocal-space accuracy. Since the $\{403\}_{\beta''}$ and $\{601\}_{\beta''}$ spots overlap with $\{200\}_{Al}$ spots, one can measure the lattice strain in the Al matrix and the misfit between β'' and Al in the same strain maps (taking care to use a small mask which does not include other β'' spots). The misfit was integrated in an area within 0.7 nm from the precipitate–matrix interface. As a control, the absolute displacement of Al columns outside precipitates was also measured.

We start off in Figure 1 by showing the misfit/displacement analysis of an example precipitate cross-section. The displacement field magnitude in (b) is found by analyzing phase changes within $\{200\}_{Al}$ Fourier space masks. The maximum magnitude is about 80 pm near the interface, which is quite significant compared to the $\{200\}_{Al}$ lattice spacing of 202 pm. Atomic columns are generally moved radially outward since β'' has a positive misfit with Al. The strain, found by spatial differentiation of the displacement, is mapped in (c). As the strain map shows a deviation in lattice parameters, the relative misfit between β'' and Al can be directly read out from inside the particle. When multiplied with the particle size, this yields the absolute misfit, which should be equal to the total displacement of Al right outside the particle (how much extra space the β'' phase takes up equals how much the lattice is displaced). The total displacement was measured as the sum of displacement on the midpoint of both sides in a ($[100]_{\beta''}$) and c ($[001]_{\beta''}$) directions, as shown in (b). For the particle in Figure 1, the numbers in the a / c direction are 110 pm / 119 pm for the misfit and 107 pm / 127 pm for the displacement, which is an acceptable agreement. The absolute misfit shows quite instructively in (a) the shape change relative to either a hypothetical zero misfit precipitate or a precipitate with bulk lattice parameters.

The analysis was performed for 24 particles with 15 distinct geometries, as tabulated in Figure 2. Relative misfit values m_a and m_c are calculated as averages for each geometry. A unit of one half unit cell is used for defining the cross-section size $N_a \times N_c$, to avoid fractional numbers in the a direction [see Figure 1(a)]. Half unit cells also give a better impression of the particle shape, e.g. a 5×5 cross-section is near equal-sided. The cross-sectional area varies between 7–19 nm^2 for the 24 particles. All particles appear to extend through the entire TEM specimen, with no projectional overlap with the Al matrix. None of the particles had defects such as stacking faults or incoherent/disordered areas, but four of them had their pointy corners rounded off by loss of one half unit cell. The β''–Al misfit and the displacement of Al

atoms correspond well, with a deviation typically below 10%. The absolute misfit is typically in the range 90–150 pm in both directions.

The lattice parameters of β'', seen through the relative misfit with Al, vary substantially and are generally smaller than the average values for large particles measured by Zandbergen *et al.*: $m_a = 3.82\%$, $m_c = 5.25\%$ [2]. In particular, particles with a high aspect ratio change the shape of their unit cells, seemingly to balance the matrix displacement/strain between the two directions. This effect is highly noticeable for the particle in Figure 1, which has a similar absolute misfit in the *a* and *c* directions despite having a high aspect ratio.

In comparison with the calculated bulk β'' lattice parameters from Ref. [16] (misfit $m_a = 5.08\%$, $m_c = 5.92\%$), the internal strain in the β'' particles is mostly compressive, and averages at around −2%. This is similar in magnitude to what is measured in the surrounding matrix, so it would appear that fcc–Al and the β'' phase are equally strainable. This agrees with computational results [16], which says that the elastic parameters of β'' and Al are quite similar in all directions. The bulk modulus of β'' is 65 GPa [19], almost the same as the 70 GPa of Al.

From the results behind Figure 2, we obtain for all precipitates the ratio between relative misfit in the *a* and *c* directions, and the ratio between physical size in the same directions, to make the scatter plot in Figure 3(a). The length and misfit ratios are close to inversely proportional (dashed line). The Poisson effect is apparent: a precipitate which is long in the *a* direction will be strongly compressed in this direction by the Al matrix, and must be expanded in the *c* direction. Interestingly, the misfit is perfectly symmetric between the *a* and *c* directions (a 4×6 particle would have the inverse misfit ratio of a 6×4 particle) even though most precipitates naturally grow to a length ratio $R_L > 1$. Recent computational results from combined density functional theory (DFT) and finite element modelling (FEM) are included in Figure 3(a) for comparison. The elastic behavior corresponds nicely with calculated results for stoichiometric $Mg_5Al_2Si_4$ particles (Al on Si_3 sites) of different shapes ($N_a = 4,8$; $N_c = 4,8$ [15]). Meanwhile, the classically assumed composition Mg_5Si_6 [2] suggests a lower *a*-misfit than the experimental data and falls outside the general trend. $Mg_4Al_3Si_4$ (Al on Si_3+Mg_1 sites) also has a good fit to the data, but has been shown to be less stable than the other two compositions in a full DFT simulation [6].

While aspect ratio is crucial, precipitate size does not appear to affect the lattice parameters, which means that the total misfit strain increases proportionally with size (until the particle loses coherency). Consequentially, as seen in Figure 3(b), the misfit area of a precipitate is roughly proportional to its total area. A linear fit was used to find the average relative misfit area of 7.18% (per equivalent undistorted Al matrix area). This is equal to the misfit *volume* since the *b* direction misfit is zero. The experimental misfit area systematically exceeds the calculated numbers for the $Mg_5Al_2Si_4$ composition from Ref. [15]. At this point it is important to keep in mind what is actually measured in maps such as Figure 1(c): not strain, but change in lattice parameters. In interpreting this as strain, we make an implicit assumption that both the matrix and the precipitate phase always retain the same atomic structure. Assuming both the current STEM results and the computational results in Refs. [15,16] to be descriptive of reality, they may be reconciled if vacancies accumulate in the matrix outside the precipitates, allowing a greater volume expansion of the β'' phase. As mentioned in the introduction, this can act as a strain relief mechanism. On the other hand, a full DFT calculation, which may be more accurate, have given a misfit area of 7.45% for a 4×4 particle of composition $Mg_5Al_2Si_4$, and a misfit area of 6.77% for a corresponding Mg_5Si_6 particle [6], in better agreement with the experimental data. This time it is $Mg_4Al_3Si_4$ that falls outside the trend. In summary, DFT-based calculations have the best overall fit with our measurement if a composition $Mg_5Al_2Si_4$ is assumed.

We give a final note on temperature dependence. Precipitates form in an environment of elevated temperature, in this case 195 °C. They will minimize their enthalpy, including strain

energy, at this temperature. The thermal contraction of Al from furnace to room temperature is 0.4% [20]. No corresponding number can be deduced for β'' at present, but if the contraction is substantially different, the effect could be measurable with the current method. With a stable specimen-heating system [21,22], strain mapping at aging temperatures can be performed to investigate the matter.

With the aid of high-resolution drift- and distortion-corrected ADF-STEM images, we have accurately measured the misfit between the Al matrix and the coherent β'' precipitate phase in an Al–Mg–Si alloy. The misfit in the different directions is highly dependent on the shape of the precipitate cross-section, suggesting that the β'' phase has a significantly elastic atomic structure. Measured misfit ratios correspond well with ratios calculated by combined DFT/FEM using a composition of $Al_2Mg_5Si_4$. The measured misfit volume has an excellent agreement with a full DFT simulation using the same composition. The lattice parameters of β'' are essentially constant with increasing cross-section size. Using an experimental high-precision technique for measuring relative distances, and comparing with state-of-the-art numerical simulations, we have demonstrated the trustworthiness of both methods, and provided new indications regarding the atomics of the β'' phase.

Acknowledgements

References

[1] J.D. Verhoeven, Fundamentals of physical metallurgy, Wiley, 1975.
[2] H.W. Zandbergen, S.J. Andersen, J. Jansen, *Science* **277** (1997) 1221–1225.
[3] S.J. Andersen, H.W. Zandbergen, J. Jansen, C. Træholt, U. Tundal, O. Reiso, *Acta Mater.* **46** (1998) 3283–3298.
[4] J.H. Chen, E. Costan, M.A. van Huis, Q. Xu, H.W. Zandbergen, *Science* **312** (2006) 416–419.
[5] H.S. Hasting, A.G. Frøseth, S.J. Andersen, R. Vissers, J.C. Walmsley, C.D. Marioara, F. Danoix, W. Lefebvre, R. Holmestad, *J. Appl. Phys.* **106** (2009) 123527.
[6] P.H. Ninive, O.M. Løvvik, A. Strandlie, *Metall. Mater. Trans. A* **45** (2014) 2916.
[7] S.J. Pennycook, B. Rafferty, P.D. Nellist, *Microsc. Microanal.* **6** (2000) 343–352.
[8] L. Jones, P.D. Nellist, *Microsc. Microanal.* **19** (2013) 1050–1060.
[9] L. Jones, H. Yang, T.J. Pennycook, M.S.J. Marshall, S. van Aert, N.D. Browning, M.R. Castell, P.D. Nellist, *Adv. Struct. Chem. Imaging* **1** (2015) 8.
[10] J. Douin, P. Donnadieu, F. Houdellier, *Acta Mater.* **58** (2010) 5782–5788.
[11] J.L. Hernández-Rivera, J.J. Cruz Rivera, C.G. Garay-Reyes, M. Ramos Azpeitia, I. Zúñiga-Alonso, R. Martínez-Sánchez, *Mater. Charact.* **73** (2012) 61–67.
[12] W.M. Stobbs, G.R. Purdy, *Acta Metall.* **26** (1978) 1069–1081.
[13] M.J. Hÿtch, A.M. Minor, *MRS bulletin* **39** (2014) 138–146.
[14] L. Jones, S. Wenner, M. Nord, P.H. Ninive, O.M. Løvvik, R. Holmestad, P.D. Nellist, "Nano-scale Strain Mapping and Modelling by High-accuracy ADF STEM and DFT", *Phys. Rev. Lett.* (submitted).
[15] F.J.H. Ehlers, S. Dumoulin, K. Marthinsen, R. Holmestad, *Mater. Sci. Forum* **794–796** (2014) 640–645.
[16] F.J.H. Ehlers, S. Dumoulin, R. Holmestad, *Comp. Mater. Sci.* **91** (2014) 200–210.

[17] E.A. Mørtsell, C.D. Marioara, S.J. Andersen, J. Røyset, O. Reiso, R. Holmestad, *Metall. Mater. Trans. A*, **46** (2015) 4369–4379.

[18] M.J. Hÿtch, E. Snoeck, R. Kilaas, *Ultramicroscopy* **74** (1998) 131–146.

[19] A.G. Frøseth, R. Høier, P.M. Derlet, S.J. Andersen, C.D. Marioara, *Phys. Rev. B*, **67** (2003) 224106.

[20] P. Hidnert, H.S. Krider, *J. Res. Nat. Bur. Stand.* **48** (1952) 209–220.

[21] L.F. Allard, W.C. Bigelow, M. Jose-Yacaman, D.P. Nackashi, J. Damiano, S.E. Mick, *Microsc. Res. Techn.* **72** (2009) 208–215.

[22] M.A. van Huis, N.P. Young, G. Pandraud, J.F. Creemer, D. Vanmaekelbergh, A.I. Kirkland, H.W. Zandbergen, *Adv. Mater.* **21** (2009) 4992–4995.
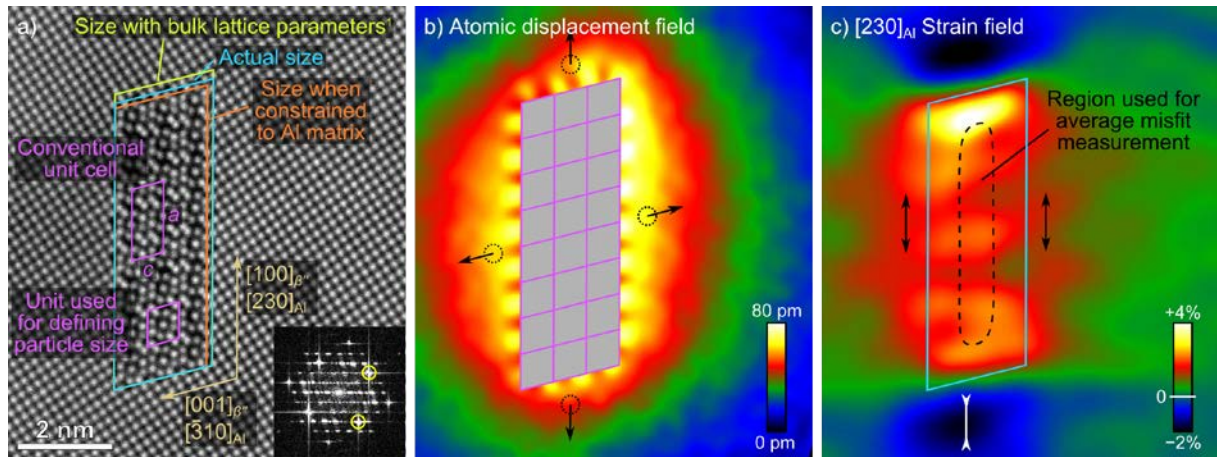
Figure 1: Analysis of an example 8×3 unit β'' precipitate. (a) Average intensity of the aligned and distortion-corrected ADF-STEM image series. Inset: Fourier transform amplitude with 1 nm GPA masks shown. (b) Displacement field magnitude in Al, with a 0.6 nm GPA mask. (c) Strain field in the $[230]_{Al} \parallel [100]_{β''}$ direction, using a 1 nm GPA mask.
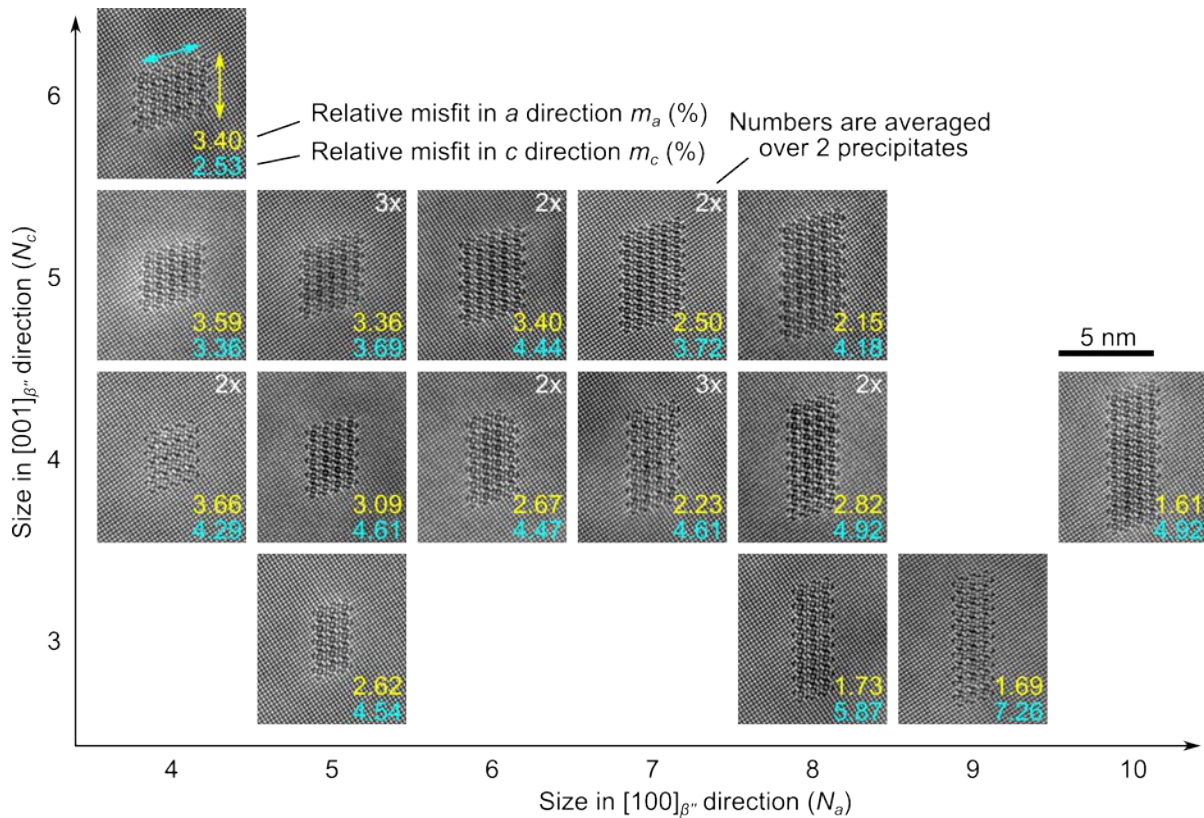
Figure 2: The collection of precipitate shapes found in this study, listing the measured misfit with Al. If more than one precipitate is found, average numbers are given. The size units are defined in Figure 1(a).
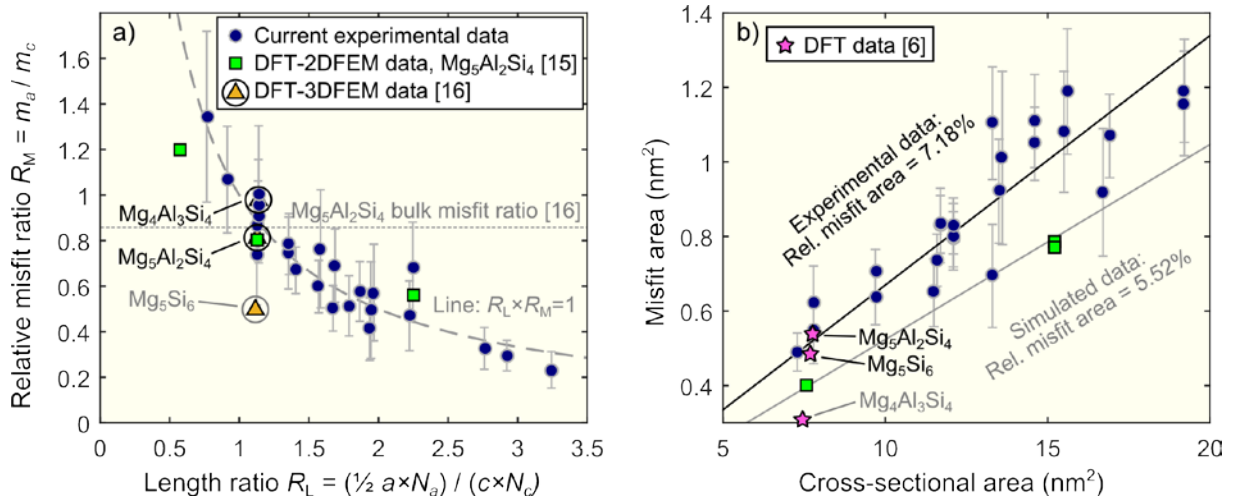

Figure 3: Plots of misfit-related properties of all the 24 precipitates. (a) Ratio between β''–Al lattice parameter misfit vs. ratio of cross-sectional side lengths. (b) Misfit area vs. total precipitate area. The error bars are calculated from standard deviations of the strain field within the measurement region [see Figure 1(c)].